

# CONFIRMATION OF THE ZERO-POINT OFFSET IN GAIA DATA RELEASE 2 PARALLAXES USING ASTEROSEISMOLOGY AND APOGEE SPECTROSCOPY IN THE *KEPLER* FIELD

JOEL C. ZINN,<sup>1</sup> MARC H. PINSONNEAULT,<sup>1</sup> DANIEL HUBER,<sup>2,3,4,5</sup> AND DENNIS STELLO<sup>6,3,4,7</sup>

<sup>1</sup>*Department of Astronomy, The Ohio State University, 140 West 18th Avenue, Columbus OH 43210, USA*

<sup>2</sup>*Institute for Astronomy, University of Hawai'i, 2680 Woodlawn Drive, Honolulu, HI 96822, USA*

<sup>3</sup>*Sydney Institute for Astronomy (SIfA), School of Physics, University of Sydney, NSW 2006, Australia*

<sup>4</sup>*Stellar Astrophysics Centre, Department of Physics and Astronomy, Aarhus University, Ny Munkegade 120, DK-8000 Aarhus C, Denmark*

<sup>5</sup>*SETI Institute, 189 Bernardo Avenue, Mountain View, CA 94043, USA*

<sup>6</sup>*School of Physics, University of New South Wales, Barker Street, Sydney, NSW 2052, Australia*

<sup>7</sup>*Center of Excellence for Astrophysics in Three Dimensions (ASTRO-3D), Australia*

## ABSTRACT

We present an independent confirmation of the zero-point offset of Gaia Data Release 2 (DR2) parallaxes using asteroseismic data of evolved stars in the *Kepler* field. Using well-characterized red giant branch (RGB) stars from the APOKASC-2 catalogue we identify a color- and magnitude-dependent zero-point offset of  $52.8 \pm 2.4(stat.) \pm 1(syst.) \mu\text{as}$ , in the sense that *Gaia* parallaxes are too small. The offset is present at nearly the same level in high and low extinction samples, and remains whether using *Gaia* DR2 or APOKASC-2 extinction estimates derived from SED fitting. The same exercise, performed with core He-burning red clump stars, yields an offset in the same sense of  $50.2 \pm 2.5(stat.) \pm 1(syst.) \mu\text{as}$ . We argue that the difference between these two measures likely reflects known systematic differences in the APOKASC-2 radius scale of RC and RGB stars at the 1% level. We recommend adopting the RGB scale because the APOKASC-2 sample was calibrated on RGB stars. Because of possible spatially-correlated parallax errors, as discussed by the *Gaia* team, our zero-point solution is specific to the *Kepler* field, but broadly compatible with the global zero-point uncertainty inferred by the *Gaia* team and independent results using Cepheids. Additionally, there is evidence for a larger absolute offset error for smaller parallaxes, which we will explore in future work.

*Keywords:* asteroseismology, catalogs, parallaxes, stars: distances

## 1. INTRODUCTION

The recent release of *Gaia* astrometry as part of Data Release 2 (Gaia Collaboration et al. 2016a, 2018) signals an unprecedented opportunity to test stellar astrophysics. In particular, the parallaxes — with typical formal precisions of 0.03mas for sources with  $G > 15$  (Lindegren et al. 2018; hereafter L18) — can be used to solve one of the biggest and most challenging problems in stellar astrophysics, namely the determination of distances. At small parallax, however, the results become sensitive to systematic errors, and checks from alternative techniques are valuable. In this paper we use asteroseismic data to test zero-point errors in the *Gaia* parallaxes.

The first data release of *Gaia*, using the Tycho-*Gaia* astrometric solution (TGAS) (Michalik et al. 2015; Gaia Collaboration et al. 2016a) represented a significant advance over the earlier *Hipparcos* work (van Leeuwen 2007a). However, the TGAS investigators did note the existence of both spatial correlations and a zero-point offset (Lindegren et al. 2016). Their work was confirmed by other investigators. For the closest objects, Jao et al. (2016) and Stassun & Torres (2016a) found consistent errors of  $\approx 0.2$ mas in the sense that TGAS parallaxes were too small when compared to trigonometric parallaxes for 612 dwarfs with parallaxes greater than 10mas, and 111 eclipsing binaries with parallaxes mostly greater than 1mas, respectively. Comparing these results for relatively nearby stars to asteroseismic parallaxes of giants with parallaxes less than 1mas indicated the presence of a fractional zero-point offset (De Ridder et al. 2016; Davies et al. 2017; Huber et al. 2017). Indeed, at larger distances than the *Kepler* (Borucki et al. 2010) giant samples, Sesar et al. (2017) found RR Lyrae parallaxes to show no indications of an offset with TGAS parallaxes, and neither did Casertano et al. (2017) among a sample of Cepheid parallaxes.

There were also follow-up tests of spatially correlated parallaxes published after TGAS. Jao et al. (2016) confirmed these spatial correlations in pointing out parallax offsets between hemispheres. Casertano et al. (2017) later reported evidence for spatial correlations in the parallax error below  $10^\circ$ . Using a larger sample, Zinn et al. (2017) mapped out the spatial correlation of the errors in the *Kepler* field below  $10^\circ$  using asteroseismic distances of  $\sim 1400$  giants, which showed structure that increased at sub-degree scales.

Systematic errors in the *Gaia* parallaxes exist, as well. Indications are that the zero-point error might best be explained by a degeneracy in the astrometric solution between a global parallax shift and a term describing a

periodic variation of the spacecraft’s basic angle<sup>1</sup> with a period of the spacecraft spin period (L18). A smaller contribution might arise from smearing of the PSF in the across-scan direction (L18). As part of the DR2 release, Arenou et al. (2018) computed the zero-point error for many populations of objects, including dwarf galaxies, classical pulsators, stars in spectroscopic surveys, and open and globular clusters (see their Table 1). The zero-point does vary among these sources, which may represent genuine variation or various systematic errors in the comparison parallaxes.

Riess et al. (2018) has confirmed an offset of  $46 \pm 13 \mu\text{as}$  for parallaxes in *Gaia* by comparing *Gaia* parallaxes to those of a sample of 50 Cepheids, whose distances can be precisely determined using a period-luminosity relation. This particular sample is redder and brighter than the sample of quasars used in L18 to test the parallax systematics, and may indeed have a genuinely different zero-point error due to trends with color and magnitude noted in L18.

The *Gaia* team has quantified the parallax error budget in DR2, with an estimate for both a global zero-point error of  $29 \mu\text{as}$  (in the sense that *Gaia* parallaxes are too small) and a spatial covariance of the parallaxes, which have a typical angular scale of ten degrees and an error of  $10 \mu\text{as}$ , which increases exponentially for smaller scales. Crucially, this means that one cannot benefit from a  $\sqrt{N}$  reduction in statistical errors of the parallax. Given these systematics, the *Gaia* team recommends adopting an irreducible systematic error on the parallaxes of  $\sim 0.1$ mas that takes into account both zero-point and spatially-correlated errors. This recommended systematic error is large enough to marginalize over much of the position-, color- and magnitude-dependent nature of the systematics, and in that sense is likely larger than the systematics particular to a specific dataset and region of the sky.

Because of the large body of research performed in the *Kepler* field, it is of great interest to quantify the particular systematic errors among its giant population. Here, we quantify the zero-point error with a sample of nearly 3500 giants with precise asteroseismic distances in the *Kepler* field that also have *Gaia* parameters.

## 2. DATA

### 2.1. The asteroseismic comparison sample

Solar-like oscillations have been detected in thousands of evolved stars by the *CoRoT* and *Kepler* missions

<sup>1</sup> The angle between the two fields of view of *Gaia* that allows an absolute measure of parallax. See Gaia Collaboration et al. (2016b) for a review of the mission design.

(Hekker et al. 2009; De Ridder et al. 2009; Bedding et al. 2010; Stello et al. 2013; Yu et al. 2018). The overall properties of the oscillation frequencies can be characterized by two global measurements: the frequency of maximum power,  $\nu_{\max}$ , and the large frequency spacing  $\Delta\nu$ . The observed frequency of maximum power is related to both the surface gravity and  $T_{\text{eff}}$  (Kjeldsen & Bedding 1995; Brown et al. 1991), while it can be demonstrated that the square of  $\Delta\nu$  is proportional to the mean density in the limiting case of homology and large radial order,  $n$  (Ulrich 1986). We can therefore solve for stellar mass and radius separately through the usage of scaling relations, typically measured relative to the Sun, if we have asteroseismic data and a robust effective temperature indicator.

Asteroseismic distance estimates are then possible because the combination of radius and  $T_{\text{eff}}$  yields a luminosity. When combined with an apparent magnitude, an appropriate set of bolometric corrections, and an extinction, the distance can be derived. In the *Kepler* field, there is uniform spectroscopic data from the APOGEE survey of the Sloan Digital Sky Survey (SDSS). Almost all of the asteroseismic targets have photometry from 2MASS (Skrutskie et al. 2006), WISE (Wright et al. 2010), and *griz* photometry from the *Kepler* Input Catalog (Brown et al. 2011) as corrected by Pinsonneault et al. (2012) to be on the SDSS system, and for which uncertainties are estimated to be 1% in  $g$  and  $r$ . The spectroscopic  $T_{\text{eff}}$  values from APOGEE that we use are calibrated to be in agreement with the Infrared Flux Method (IRFM) photometric scale of González Hernández & Bonifacio (2009) for targets in low extinction fields. The extinctions are well-studied in the *Kepler* fields, because they can be inferred by requiring consistency between photometric and spectroscopic temperature estimates (see Rodrigues et al. 2017, for details on Bayesian fitting of the extinctions used in the APOKASC-2 catalogue). The bolometric corrections are not expected to dominate the error budget.

Our sample of 6676 evolved *Kepler* stars with asteroseismic and spectroscopic data is taken from Pinsonneault et al. (2018), hereafter APOKASC-2. The APOKASC-2 study provides asteroseismic evolutionary state classification, masses, radii, and extinction measures in the V-band.

The masses and radii of shell H-burning (hereafter RGB) stars are calibrated against fundamental data in star clusters, with typical random errors in radius of under 2% and well-controlled systematics. APOKASC-2 uses theoretically-motivated corrections to the  $\Delta\nu$  scaling relation (e.g., White et al. 2011; Sharma et al. 2016), which induce a differential change between the radii and

masses of RGB stars and core He-burning, or RC stars. As a result, it is important to analyze RGB and RC stars separately, as there are known effects that can produce relative offsets between the two populations (e.g., Miglio et al. 2012). The relative radii of both are consistent with one another in open clusters in the *Kepler* field, but differences at the few percent levels could not be ruled out using those samples alone. Our basic sample therefore consists of 3475 RGB stars and 2587 RC stars which pass the *Gaia* DR2 selection cuts as described below. Unless otherwise noted, we only use first-ascent red giants in our main analysis because the APOKASC-2 radii are directly calibrated against RGB stars in open clusters, and because of their larger dynamic range in parameter space — radius and luminosity, in particular — compared to RC stars.

Extinction can vary across the 10 degree-wide *Kepler* field. To investigate whether our results depend on extinction, we divide our data into sub-samples below and above  $b = 15^\circ$ . There is also a high-extinction region in the *Kepler* field at  $\ell \lesssim 73^\circ$ , which we also consider a high-extinction region for our validation tests.

## 2.2. The *Gaia* Data Release 2 sample

The DR2 catalogue contains a host of useful astrometric, photometric, and derived quantities for our purposes. In addition to the parallaxes,  $\varpi_{\text{Gaia}}$ , we take the *Gaia* magnitude in the G-band,  $G$ , and the astrometric pseudo color,  $\nu_{\text{eff}}^2$ , for use as explanatory factors in our model to describe the offset between asteroseismic and *Gaia* parallaxes. We also make use of stellar radii,  $R_{\text{Gaia}}$ , effective temperature, and extinction in the *Gaia* G-band,  $A_G$ , which have all been computed using Apsis (Bailer-Jones et al. 2013; see Andrae et al. 2018 for details on using Apsis in deriving DR2 stellar parameters).

We only use stars in common with APOKASC-2 and DR2 by matching on 2MASS ID, and from those, only keep those that meet criteria used by Andrae et al. (2018), namely:

- `astrometric_excess_noise` = 0
- `visibility_periods_used` > 8

and with  $\chi^2 \equiv \text{astrometric\_chi2\_al}$ ,  $n \equiv \text{astrometric\_n\_good\_obs\_al} - 5$ ,  $GBP = \text{phot\_bp\_mean\_mag}$ ,  $GRP = \text{phot\_rp\_mean\_mag}$ ,

- $\chi \equiv \sqrt{\chi^2/n}$ ,  $\chi < 1.2\max(1, \exp -0.2(G - 19.5))$

<sup>2</sup> An astrometrically-determined color term estimated as an extra parameter in the otherwise five-parameter astrometric solution (see §3.1 of L18).

$$\bullet 1.0 + 0.015(GBP - GRP)^2 < \text{phot\_bp\_rp\_excess\_factor} < 1.3 + 0.06(GBP - GRP)^2$$

These quality cuts ensure a good astrometric solution. We also exclude a handful of stars whose parallaxes or radii that we derive below disagree between asteroseismology and *Gaia* at the  $5\sigma$  level. We do not explicitly exclude negative parallaxes, and our analysis method described in the next section does not require positive parallaxes. However, after the above cuts, only positive parallaxes remain.

### 3. METHODS

A star’s radius,  $R$ , is related to its parallax,  $\varpi$ , through its effective temperature,  $T_{\text{eff}}$ , and its bolometric flux,  $F$  via

$$\begin{aligned} \varpi(T_{\text{eff}}, F) &= F^{1/2} \sigma_{\text{SB}}^{-1/2} T_{\text{eff}}^{-2} R^{-1} \\ &= f_0^{1/2} 10^{-1/5(m+BC-A_m)} \sigma_{\text{SB}}^{-1/2} T_{\text{eff}}^{-2} R^{-1}, \end{aligned} \quad (1)$$

$$(2)$$

where  $\sigma_{\text{SB}}$  is the Stefan-Boltzmann constant,  $f_0$  is a zero-point factor to convert magnitude to flux,  $BC$  is the bolometric correction, which depends on magnitude,  $m$ , and  $A_m$  is the extinction in that band. One may use this equation to compute a radius from the *Gaia* parallax, or a parallax from an asteroseismic radius. Asteroseismic radii themselves are derived from a radius scaling relation using the asteroseismic properties  $\Delta\nu$  and  $\nu_{\text{max}}$ , which represent the typical frequency spacings between acoustic overtone modes in solar-like oscillators and the frequency for which those oscillations are largest:

$$(R/R_{\odot}) \approx (\nu_{\text{max}}/\nu_{\text{max},\odot})(\Delta\nu/\Delta\nu_{\odot})^{-2}(T_{\text{eff}}/T_{\text{eff},\odot})^{1/2}. \quad (3)$$

The published *Gaia* radii depend on an estimate of the flux of the star, and not just the parallax. Because the published *Gaia* radii are computed without taking into account extinction, the published *Gaia* radii are systematically too small. To remove this known effect, we calculate our own radii using *Gaia* parallaxes, according to Equation 1 with visual photometry, which we will refer to henceforth as *Gaia* radii.

One can see that Equation 1 suggests that for our comparison between *Gaia* and seismic results, we can either use *Gaia* parallaxes with a flux and a temperature to yield a *Gaia* radius, or alternately use the asteroseismic radius along with a flux and temperature to compute a parallax. In the following, we consider both approaches.

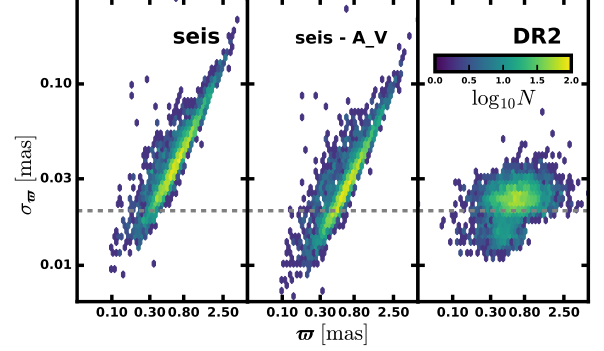


**Figure 1:** Parallax errors as a function of asteroseismic parallax with and without  $A_V$  errors (“seis”, “seis- $A_V$ ”) and *Gaia* parallax for our main sample. The color scale indicates the number of points per hexagonal cell. The horizontal dashed line indicates an error of 0.02mas, to guide the eye. Note the logarithmic scale on both axes.

#### 3.1. Parallax comparison

It is simplest to identify a zero-point offset in the *Gaia* parallaxes in parallax space—i.e., by converting asteroseismic radii into asteroseismic parallaxes. The following equations represent our assumptions that 1) the true asteroseismic parallax,  $\varpi_{\text{seis}}$ , and the true *Gaia* parallax,  $\varpi_{\text{Gaia}}$ , are one in the same; 2) the *observed* *Gaia* parallaxes are offset from the true parallax by a constant value,  $c$ , and are subject to measurement/modelling noise; 3) the *observed* asteroseismic radii are unbiased measurements of the true parallax, subject to noise:

$$\varpi_{\text{seis}} = \varpi_{\text{Gaia}} \quad (4)$$

$$\hat{\varpi}_{\text{Gaia}} = \varpi_{\text{Gaia}} + c + \epsilon_{\varpi_{\text{Gaia}}} \quad (5)$$

$$\hat{\varpi}_{\text{seis}} = \varpi_{\text{seis}} + \epsilon_{\varpi_{\text{seis}}}, \quad (6)$$

where a hatted quantity indicates an observed quantity and the un-hatted quantity is the true value for that quantity. The variance due to measurement/modelling noise in the observed asteroseismic and *Gaia* radii are simply the variance of the random variates  $\epsilon_{\varpi_{\text{seis}}}$  and  $\epsilon_{\varpi_{\text{Gaia}}}$ , which we denote as  $\sigma_{\varpi_{\text{seis}}}^2$  and  $\sigma_{\varpi_{\text{Gaia}}}^2$ . In our analysis, we ignore objects that were  $5\sigma$  outliers in parallax difference.

The dominant assumption in our analysis is that the asteroseismic parallax/radius scale is the absolute one, and the *Gaia* parallax/radius scale deviates therefrom. Although our result’s error budget benefits from the precision of the asteroseismic sample, it is not necessary for our sample to have more precise parallaxes than that of *Gaia*. If taken at face value, Figure 1 demonstrates that the *Gaia* parallaxes for our sample are at least as pre-

cise as that of the asteroseismic parallaxes, if not more. In fact, we may have reason to suspect that the *Gaia* parallax errors are artificially too low. For stars with  $G < 12$ , the errors appear well-behaved, thanks to a post-processing inflation to the formal uncertainties the *Gaia* team applied (L18). However, through comparisons to literature distances, Arenou et al. (2018) has pointed out that parallax errors are significantly underestimated, by as much as 40% for  $13 < G < 15$  (the regime in which 15% of our sample lives). For the purposes of our analysis, we have assumed that the formal errors on *Gaia* parallaxes are accurate. We also have reason to suspect that the  $A_V$  errors are inflated, which boosts the asteroseismic parallax errors (“astero” versus “astero - A\_V” in Figure 1). Indeed, we find that a larger formal  $A_V$  error does not correspondingly increase *Gaia* radius scatter around the more precise asteroseismic radii. We will investigate the impact of the formal uncertainty of  $A_V$  and spatial correlations thereof on the *Gaia* radius budget in forthcoming work, and for now assume the Bayesian error estimates of  $A_V$  from Rodrigues et al. (2017).

Whether or not the *Gaia* parallax uncertainties in Figure 1 represent true statistical uncertainties or not, the inferred value for the parallax offset we report does not rest on the asteroseismic sample’s *precision*, though it does rest on the assumption that the asteroseismic parallaxes are *accurate*, which we discuss further in §5.

We find that the goodness-of-fit of the model depends crucially on allowing for spatially-correlated errors according to the estimate for the spatial covariance matrix of the *Gaia* parallaxes in Eq. 16 of L18. We write the covariance between two stars  $i$  and  $j$  separated by an angular distance,  $\theta_{ij}$  as  $C_{ij}(\theta_{ij}) = f(\theta_{ij}) + \delta_{ij}\sigma^2\varpi_{Gaia}$ , where  $f(\theta_{ij})$  describes the spatial correlations in parallax error, and  $\delta_{ij}$  is the Kronecker delta function. L18, using their quasar reference sample, find  $f(\theta_{ij}) = a\exp(-\theta_{ij}/b)$ , with  $a = 135\mu\text{as}^2$  and  $b = 14^\circ$ . This covariance function was fitted across the entire sky, and models well the covariance at the largest scales. However, because we want to characterize the zero-point error in the *Kepler* field specifically, we can ignore the covariance at the largest scales, and only consider the covariance on scales smaller than the *Kepler* field. We tried three approaches for quantifying the small-scale spatial correlations: 1) Adopting the exponential form from L18 as is ( $a = 135\mu\text{as}^2$  and  $b = 14^\circ$ ); 2) Adopting the same exponential form from L18, but with  $a = 1500\mu\text{as}^2$  and  $b = 0.11^\circ$  (the angular scale is taken from fits to TGAS parallax covariance from Zinn et al. (2017), and  $a$  is chosen to reproduce the smallest-scale behavior in the observed covariance in L18); and 3) ignoring spatial cor-

relations altogether. We settle on the L18 covariance function (1), as it yields the best goodness-of-fit, and consider the average spread of the best-fitting  $c$  among these methods as a systematic error on  $c$  of  $\pm 1\mu\text{as}$ .

Conveniently, the *Kepler* field is easily sub-divided into small patches that correspond to the spacecraft “modules” that house the CCDs on which a star’s image is recorded for a given quarter<sup>3</sup>. We choose therefore to consider the errors on the parallax for stars of a given module to be independent of those of stars on every other module. As we are ignoring correlations in parallax on the largest scales, this is justified, and amounts to truncating our covariance function at angular scales larger than the module size of  $\sim 2.4^\circ$ . This choice is equivalent to ignoring errors on our inferred zero-point offset due to the fact that the zero-point could be different for the same population of giants in a different, *Kepler*-sized field in another location on the sky.

Ignoring correlations among the observables ( $T_{\text{eff}}$ ,  $\Delta\nu$ ,  $\nu_{\text{max}}$ ,  $A_V$ ,  $g$ , and  $r$ ) yields a likelihood function for  $N$  stars on each module,  $m$ :

$$\begin{aligned} \mathcal{L}_m(c|\{\hat{\varpi}_{Gaia}\}, \{\hat{F}\}, \{\hat{T}_{\text{eff}}\}, \{\hat{\Delta\nu}\}, \{\hat{\nu}_{\text{max}}\}, \{\hat{A}_V\}, \\ \{\hat{g}\}, \{\hat{r}\}) = \frac{1}{\sqrt{(2\pi)^N|C|}} \\ \exp -\frac{1}{2}(\vec{y} - \vec{x})^T C^{-1}(\vec{y} - \vec{x}), \end{aligned} \quad (7)$$

where

$$\begin{aligned} \vec{y} &\equiv \hat{\varpi}_{\text{seis}}(\hat{T}_{\text{eff}}, \hat{\Delta\nu}, \hat{\nu}_{\text{max}}, \hat{A}_V, \hat{g}, \hat{r}, \hat{BC}) \\ \vec{x} &\equiv \hat{\varpi}_{Gaia} + c, \end{aligned}$$

and where  $F$  has been computed using  $g$  and  $r$  in combination with  $A_V$  and a V-band bolometric correction that depends on  $T_{\text{eff}}$  from Flower (1996),  $BC(T_{\text{eff}})$ , on which we assign a 3% uncertainty. The conversion from  $g$  and  $r$  to a V-band magnitude is taken from Lupton 2005<sup>4</sup>. The error introduced from the transformation is negligible compared to the uncertainties on  $A_V$ , given the 1% errors on  $g$  and  $r$ .

Because L18 points out color and magnitude dependences of the parallax zero-point error among their comparison quasar sample, we build upon this model by adding *Gaia* color and magnitude terms:

<sup>3</sup> The spacecraft turns by  $90^\circ$  each quarter, so the same star is found on one of four modules over the 16-quarter *Kepler* mission

<sup>4</sup> <http://www.sdss3.org/dr8/algorithms/sdssUBVRITransform.php>

$$\begin{aligned}
P_m(c, d, e | \{\hat{\omega}_{Gaia}\}, \{\hat{F}\}, \{\hat{T}_{\text{eff}}\}, \{\hat{\Delta}\nu\}, \{\hat{\nu}_{\text{max}}\}, \{\hat{A}_V\}, \\
\{\hat{g}\}, \{\hat{r}\}, \{\hat{G}\}, \{\hat{\nu}_{\text{eff}}\}) \propto \\
\exp\left(-\frac{1}{2}[c - \bar{c}]^2/\sigma_c^2/M\right) \\
\frac{1}{\sqrt{(2\pi)^N |C'|}} \exp\left(-\frac{1}{2}(\vec{y} - \vec{x})^T C^{-1}(\vec{y} - \vec{x})\right),
\end{aligned} \tag{8}$$

where

$$\begin{aligned}
\vec{y} &\equiv \hat{\omega}_{\text{seis}}(\hat{T}_{\text{eff}}, \hat{\Delta}\nu, \hat{\nu}_{\text{max}}, \hat{A}_V, \hat{g}, \hat{r}) \\
\vec{x} &\equiv \hat{\omega}_{Gaia} + c + d(\hat{\nu}_{\text{eff}} - \bar{d}) + e(\hat{G} - \bar{e}).
\end{aligned}$$

This is our preferred model, which describes the Bayesian posterior probability of the parameters  $\mu_m \equiv \{c, d, e\}$ , for each module,  $m$ , out of a total of  $M = 21$  modules. We use a prior on  $c$  based on our best-fitting value for the model with no color or magnitude terms or spatial correlations in parallax,  $\bar{c} \approx 55\mu\text{as}$ , and a width approximately twice its uncertainty,  $\sigma_c \approx 1.5\mu\text{as}$ , as reported in the next section, though our results are insensitive to including the prior or having an implicit, flat, improper prior for  $c$ . Here, the covariance includes two additional terms along the diagonal:  $C'_{ij} = C_{ij} + \delta_{ij}\sigma_{\nu_{\text{eff}}}^2 + \delta_{ij}\sigma_G^2$ , with  $\sigma_G$  the error on  $G$ , which we assign as 1%, and  $\sigma_{\nu_{\text{eff}}}$  as the `astrometric_pseudo_colour_error` field from the DR2 catalogue. We assign  $\bar{d} \approx 1.5$  and  $\bar{e} \approx 12.2$  to be the medians of  $G$  and  $\nu_{\text{eff}}$  for our sample. They are therefore not parameters in this model. We have used the astrometric source color here as it should be more correlated with the astrometric properties of the *Gaia* DR2 solution than *GBP-GRP*. Arenou et al. (2018) indeed finds that the *Gaia* quasar parallax zero-point is more sensitive to  $\nu_{\text{eff}}$  than *GBP-GRP* (see their Figure 18).

Because we can consider each module independently, we estimate  $c$  for each module, and combine their values assuming they are described by a Gaussian around true values, estimated to be  $\hat{\mu}_M$ , with covariance,  $\hat{\Sigma}_M$ , which we estimate as:

$$P_M(c, d, e) \propto \Pi_{m=0}^M P_m(c, d, e) \propto \mathcal{N}(\hat{\mu}_M, \hat{\Sigma}_M), \tag{9}$$

where

$$\hat{\Sigma}_M = \left( \sum_{m=0}^M \hat{\Sigma}_m^{-1} \right)^{-1} \tag{10}$$

$$\hat{\mu}_M = \hat{\Sigma}_M \left( \sum_{m=0}^M \hat{\Sigma}_m^{-1} \hat{\mu}_m \right), \tag{11}$$

where each module's best-fitting parameters,  $\hat{\mu}_M$ , and covariance matrices,  $\hat{\Sigma}_m$ , are estimated from MCMC chains from `emcee` (see Neiswanger et al. 2013, for this and other more elaborate MCMC parallelization procedures).

### 3.2. Radius comparison

We also compute the offset in inverse radius space. In this case the error budget is allocated differently because the *Gaia* radius inherits uncertainty from combining  $\varpi_{Gaia}$  with the flux and temperature to yield a radius.

We opt to work in terms of inverse radius, which is directly proportional to parallax, thereby avoiding the bias and high variance when converting the parallax to a distance with  $d = 1/\varpi$ . We refer the reader to Bailer-Jones (2015) for thorough discussions of the pitfalls in the naive (non-inverted) distance approach. This inverted radius formalism also does not require the parallax to be positive, as a negative parallax indicates a noisy estimate of a large radius (small inverse radius). (In our sample, however, the negative parallaxes are filtered out by the conditions listed in §2). The formal uncertainties on the asteroseismic radii  $\sim 1.5\%$ , are such that inverting the asteroseismic radius is well-tolerated.

We start out by assuming that the true asteroseismic radius  $R_{\text{seis}}^{-1}$  should equal the true *Gaia* radius,  $R_{Gaia}^{-1}$ .

$$R_{\text{seis}}^{-1} = R_{Gaia}^{-1} \tag{12}$$

$$\hat{R}_{Gaia}^{-1} = F^{-1/2} T_{\text{eff}}^2 (\varpi + c) + \epsilon_G \tag{13}$$

$$\hat{R}_{\text{seis}}^{-1} = R_{\text{seis}}^{-1} + \epsilon_s \tag{14}$$

$$\tag{15}$$

where a hat denotes an observed quantity and the variances of the noise parameters for  $\epsilon_s$  and  $\epsilon_G$  are denoted  $\sigma_s^2$  and  $\sigma_G^2$ .

Assuming no intrinsic scatter in the parallax offset for the *Kepler* field, we can formulate Equation 12 into a likelihood for our  $N$  stars, assuming the observables are all normal variates with formal uncertainties described by  $\hat{x} = x + \epsilon_x$ :

$$\begin{aligned}
\mathcal{L}(c | \{\varpi_{Gaia}\}, \{\hat{F}\}, \{\hat{T}_{\text{eff}}\}, \{\hat{\Delta}\nu\}, \{\hat{\nu}_{\text{max}}\}, \{\hat{A}_V\}, \{\hat{g}\}, \{\hat{r}\}) = \\
\Pi_i (2\pi)^{-N/2} (\sigma_{FT,i}^2 + \sigma_{s,i}^2 + \sigma_{G,i}^2)^{-1/2} \\
\exp\left(-\frac{1}{2}(x_i - y_i)\right),
\end{aligned} \tag{16}$$

where

$$x_i \equiv R_{\text{seis},i}^{-1}(\hat{\Delta\nu}, \hat{\nu}_{\text{max}}, \hat{T}_{\text{eff}})$$

$$y_i \equiv \hat{R}_{\text{Gaia},i}^{-1}(\hat{\varpi}_{\text{Gaia}}, \hat{F}, \hat{T}_{\text{eff}}, \hat{A}_V, \hat{g}, \hat{r}) + c\hat{F}^{-1/2}\hat{T}^2,$$

and where  $\sigma_{\hat{F}T,i}^2$  is the formal variance of the quantity  $\hat{F}^{-1/2}\hat{T}^2$ . Again, we ignore correlations among observables (notably in temperature). This model is used for validating our main model, Equation 8. We do not include spatial correlations in the parallax, and neither do we fit for color or magnitude terms in radius space.

#### 4. RESULTS

We report the uncertainty in  $c$ ,  $d$ , and  $e$  from the diagonal of the parameter covariance matrix described above,  $\hat{\Sigma}_M$ , and the best-fitting values from  $\hat{\mu}_M$ , except for the radius space comparison offset,  $c$ , (Equation 16), where we take the mean and standard deviation from our MCMC chains.

##### 4.1. Parallax and radius offsets

No matter the method used, we find a consistent *Gaia* parallax zero-point error for our *Kepler* RGB sample of  $\approx 53\mu\text{as}$ . Our main RGB sample yields an offset of  $52.8 \pm 2.4(\text{stat.}) \pm 1(\text{syst.})\mu\text{as}$ , with color and magnitude terms of  $-150.7 \pm 22.7\mu\text{as}\mu\text{m}$  and  $-4.21 \pm 0.77\mu\text{as}\text{mag}^{-1}$ . This result is consistent with that inferred from the radius-based method ( $c = 56.3 \pm 0.65\mu\text{as}$ ), when fitting  $c$  without the color and magnitude terms ( $c = 52.9 \pm 0.35\mu\text{as}$ ), and as well as when no spatially-correlated parallax errors are used ( $c = 54.8 \pm 0.66\mu\text{as}$ ).

We visualize the offset in parallax in Figure 2, which shows evidence of a parallax-dependent offset, even when accounting for color and magnitude terms. In particular, there seems to be an up-tick of the offset for  $\varpi_{\text{Gaia}} \lesssim 0.2\text{mas}$ . Crucially, the same trend is *not* seen in Figure 3b, which is plotted as a function of the astero-seismic parallax. We interpret this as evidence for an offset that is a function of  $\varpi_{\text{Gaia}}$ . We return to this point in §5.

##### 4.2. Systematic effects on the offset inference

We performed several checks of the offset for different populations in order to estimate any systematic effects biasing our inferred value of  $c$ , including:

1. A high-parallax sub-sample with  $\varpi_{\text{Gaia}} > 1\text{mas}$
2. A high-precision sub-sample with  $\sigma_{\varpi_{\text{Gaia}}}/\varpi_{\text{Gaia}} < 0.05$
3. Two high-extinction sub-samples ( $\ell < 73^\circ$  and  $b < 15^\circ$ )

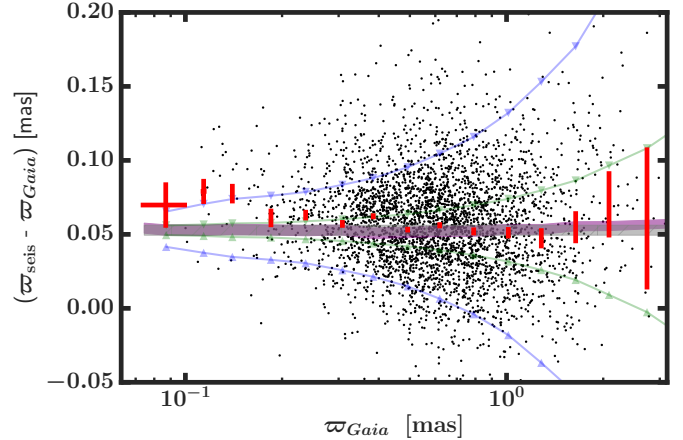


**Figure 2:** Difference in *Gaia* and astero-seismic parallax, as a function of *Gaia* parallax. The observed data are shown in black, along with a binned median (red error bars). The  $1\sigma$  region for the best-fitting model using only a constant offset of  $c$  is indicated by the grey band, and one with color and  $G$  terms to describe the *Gaia* parallax error by the purple band (with  $\pm 1\sigma$  in the constant offset, and  $\pm 0.5\sigma$  in the color and  $G$  terms). Shown also are predicted effects from errors of  $\pm 100\text{K}$  in the APOGEE temperature scale (blue) and  $\pm 2\%$  in the radius scaling relation (Equation 3; green). See text for details. There is evidence for an increase in the offset above the models for  $\varpi_{\text{Gaia}} \lesssim 0.2\text{mas}$ .

4. Two low-extinction sub-samples ( $\ell > 73^\circ$  and  $b > 15^\circ$ )
5. A sub-sample consisting only of red clump stars (RC)

In all of these cases, our parallax space model space was used to infer  $c$  (Equation 8), and only RGB stars were included (except for the RC sub-sample, which consisted exclusively of RC stars). The results of the offsets and corresponding reduced  $\chi^2$  are tabulated in Table 1. For comparison, our main sample is included as “RGB”.

#### 5. DISCUSSION

In §3, we laid out two models in parallax space: one with a constant offset, and another with additional color and  $G$ -band magnitude terms. As a function of astero-seismic parallax, we see in Figure 3 that we do not require a model with color and magnitude trends (purple band) — a simple constant offset suffices (grey band).

It is only in looking at the offset as a function of our other parameters in Figure 4 that we see the color and magnitude terms are required to explain the data. This is particularly evident of course in  $\nu_{\text{eff}}$  and  $G$  space (Figures 4e & 4f), but also notably in  $\Delta\nu$  and  $\nu_{\text{max}}$  space (Figures 4b & 4c), where the color and magnitude terms perform better than the constant offset.

### 5.1. Checks with sub-samples of the main sample

Importantly, our result does not depend on extinction, which can also be seen in Figure 4d. Indeed, the APOGEE temperature scale we have adopted is spectroscopic, and therefore insensitive to extinction, as are asteroseismic frequencies. We therefore expect our result to be independent of extinction on the asteroseismic side, but it seems so are *Gaia* parallaxes. Given the excellent agreement among our sub-samples, we are confident in our estimate of the *Gaia* parallax zero-point error for *Kepler* giants, and do not think there are significant biases in our estimate.

From Table 1, it is clear that the only differences in the inferred offset of note are in the high  $\varpi_{Gaia}$  and RC sub-samples. The lower offset for the high parallax sample is consistent with an increasing parallax zero-point error for smaller parallax, as we discuss later. Regarding the RC sub-sample, the observed parallax difference between it and the RGB sample is comparable in size to the systematic difference between red giant and red clump radii found in Pinsonneault et al. (2018). The radii in APOKASC-2 were calibrated on giant open cluster members and not clump stars, and thus there remain differential radius offsets between the red clump and the red giant branch. Given the robust calibration of radius for RGB stars, we adopt the parallax zero-point error estimated from the APOKASC-2 RGB sample.

The too-low reduced  $\chi^2$ ,  $\chi^2/dof$  for the high-precision sample, shown in Table 1, could indicate that our error budget is inadequate, though we do achieve acceptable goodness-of-fit for our other samples. Incorrect error estimates of RC radii similarly might lead to the too-low reduced  $\chi^2$  for the RC sub-sample. Finally, we note that there is uncertainty in our result due to the unknown form of the spatial covariance function for the *Kepler* field, which could bias our reduced  $\chi^2$  by changing the best-fitting value and/or changing the effective number of degrees of freedom. We will explore the latter effect in a future work.

### 5.2. Checks against *Gaia* photometry

We have also checked that the offset is present in radius space when using *Gaia* G-band magnitude and G-band extinctions. To do so, we compute a the bolometric correction according to the procedure in Andrae et al. (2018), using *Gaia* temperatures, adopting a standard propagation of uncertainty. Our uncertainty budget for *Gaia* radii computed in this way is as follows: We assign uncertainties to the bolometric fluxes based on the

effective temperature, the raw *Gaia* flux<sup>5</sup>, the G-band zero-point, and  $A_G$  via standard propagation of uncertainty, ignoring correlations between terms in the bolometric correction expression (meaning in general, our flux uncertainties will be under-estimated). We also add in quadrature an error of 2.3mmag to the G-band magnitudes, as suggested by Arenou et al. (2018). The largest source of uncertainty in the flux is the extinction uncertainty. We adopt the typical expected uncertainty on the extinction from Andrae et al. (2018) of  $\sigma_{A_G} \approx 0.46$ , which can lead to many tens of percent uncertainties on the flux. Note that we assume the  $\sigma_{A_G}$  follow a Gaussian distribution, even though, as noted in Andrae et al. (2018), the Apsis extinctions are strictly positive, meaning they do not behave as normal variates.

We use Equation 16, except instead of using a V-band magnitude,  $A_V$ , and a visual bolometric correction, we use the G-band magnitude,  $A_G$ , and a G-band bolometric correction. The results are in tension with the visual photometry estimate, with  $c = 71.6 \pm 0.34 \pm 1 \mu\text{as}$ . Given the caveats indicated in Andrae et al. (2018) for using  $A_G$  as is, we do not think this is a meaningful difference in offsets. It is possible that the fact the visual and G-band bolometric corrections were inferred from different underlying data could lead to systematically different values for our giant sample. The non-normal errors on  $A_G$  could also contribute to the difference.

### 5.3. Fidelity of the APOGEE temperature scale and the radius scaling relation

We show in Figures 2, 3 and 4 what the offset between asteroseismology and *Gaia* would be observed to be if the APOGEE temperature scale differed by  $+100K$  (blue lines with upward triangles) and  $-100K$  (blue lines with downward triangles), and if the asteroseismic radii were inflated by 2% (green lines with upward triangles) and deflated by 2% (green lines with downward triangles). In other words, they indicate what the binned median (red error bars) would look like if the APOGEE temperatures or scaling relations were responsible for the observed offsets. We see that these systematic effects appear to be degenerate with a shift in the zero-point error, as the lines are either above or below the fiducial models in grey and purple bands. In detail, the observed parallax zero-point error is not consistent with errors in temperature or the radius scaling relation, however. We

<sup>5</sup> Evans et al. (2018) describes a revision to the G-band photometric zero-point,  $f_0$ , based on updated G-band transmission curves. This correction mostly affects the red passband, though the G passband flux is revised down by  $\approx 0.3\%$ . We apply this correction, and factor in the revised uncertainty of the zero-point  $\sigma_{ZP, REV} = 0.0011$ , according to Table 1 in Evans et al. (2018).



will consider as an example the model for the effect of an increase in the radius (green upward triangles), e.g., due to a correction to the scaling relations that resulted in the radii increasing. In this case, the offset between *Gaia* and asteroseismic radii would decrease when viewed as a function of temperature because larger radii, at fixed flux and temperature, imply the stars must be farther away and thus have a smaller parallax, shifting asteroseismic parallaxes closer to the observed *Gaia* parallaxes (Figure 4a). On the other hand, when the effect of an increase in radius is viewed as a function of magnitude, the brightest stars experience the largest decrement in asteroseismic parallax — a population effect whereby the brightest stars in APOKASC-2 are the closest (largest parallax) — meaning that a fractional increase in radius for these stars leads to the largest absolute parallax shift. This is in the *opposite* sense of the observed trends (i.e., we observe the offset to *increase* for brighter stars). Looking at the trends in all of these dimensions in this way, there does not seem to be evidence for global problems in the temperature or APOKASC-2 radius scale that would cause the *Gaia* zero-point error we infer.

Indeed, we also do not find evidence of temperature and scaling relation scale effects in radius or asteroseismic parallax space. If APOKASC-2 observables were the root cause of the observed differences between parallax scales, we would expect the difference to be a function of asteroseismic parallax, as the temperature (blue lines) and scaling relation (green lines) effects shown in Figure 3b, which are fractional, would become more severe for larger parallax. This is even clearer in Figure 3a, where the *fractional* radius difference is shown. Here, the slope in the fractional radius difference cannot be caused by either temperature or scaling relation problems Figure 3b — it can only be moved up and down by the fractional error induced in temperature or radius.

As a final word on the matter, we note that the above statements have assumed that any changes to the observed parallax offset by radius scaling relation errors are present at all radii (a constant fractional error). As we describe in the next section, however, we expect the giants with the largest radii to have stronger breakdowns in scaling relations than their less-evolved counterparts. Intriguingly, we see a decrease in the parallax offset for  $\varpi_{\text{seis}} \lesssim 0.3\text{mas}$  (unlike the up-tick in the offset as a function of *Gaia* parallax,  $\varpi_{\text{Gaia}}$ , discussed more in §5.4), which would be in the correct sense for asteroseismic radii being too large (parallaxes too small) only for the largest giants (found at the largest distance/smallest parallax). This effect would also manifest as a decrease in the parallax offset for low- $\Delta\nu$  and  $\nu_{\text{max}}$  stars. We do see hints of this in Figures 4b & c, where there is

a down-tick in the parallax difference for  $\Delta\nu \lesssim 1\mu\text{Hz}$  and  $\nu_{\text{max}} \lesssim 1\mu\text{Hz}$ . Given the expectation that larger giants would have a stronger breakdown in the radius scaling relation, it might also explain the flattening of the slope in fractional radius difference above  $R_{\text{seis}} \sim 20R_{\odot}$ ,  $R_{\text{seis}}/R_{\text{Gaia}} - 1$ . However, because larger stars are cooler, this effect is degenerate with a non-linear *Gaia* parallax error, where indeed we see that our linear model in color space cannot describe the data for  $\nu_{\text{eff}} \lesssim 1.45$  in Figure 4e. We cannot discriminate at this point between a scaling relation problem or a color-dependent *Gaia* error term that our linear model cannot describe. We are working on a model to sort out color-dependent parallax issues in *Gaia* versus evidence for genuine scaling relation corrections. We emphasize, however, that any hints at scaling relation breakdown only concerns interpreting small residuals at the extremes (in color, radius, distance, etc.) of our APOKASC-2 parameter space. We stress that the global *Gaia* parallax error we report is not consistent with being caused by temperature or scaling relation errors.

#### 5.4. Hints of parallax-dependent offset

As we have mentioned, apart from a constant offset in the asteroseismic and *Gaia* parallax scales, we also see a trend with  $\varpi_{\text{Gaia}}$ , such that the offset increases with decreasing  $\varpi_{\text{Gaia}}$ . This is possibly a bias caused by the astrometric quality cuts we impose, which could lead to edges at the extremes of parallax space. We will investigate such effects in future work. In theory, this could also be caused by a breakdown in scaling relations, which seems to occur for more evolved — and therefore generally more distant — giants (Mosser et al. 2013; Stello et al. 2014). The largest sample of giants with asteroseismic and eclipsing binary masses and radii (10) indicate evidence for scaling relations yielding inflated masses and radii (Gaulme et al. 2016), though other results with smaller sample sizes have shown consistency in mass and radius scaling relations (Frandsen et al. 2013; Gaulme et al. 2014; Brogaard et al. 2016). Moreover, interferometric radii for four giants in Huber et al. (2012) do not show evidence for systematics in the scaling relations. Following the arguments made earlier in this section, if there were a dependence on the scaling relations, we would expect to see a flaring of the parallax difference at large asteroseismic parallax (Figure 3b), which we do not observe. Furthermore, Stassun et al., in prep have found what appears to be a parallax-dependent offset in their independent analysis using eclipsing binary parallaxes, (K. Stassun, personal communication; Stassun & Torres 2016b; Stassun et al.,

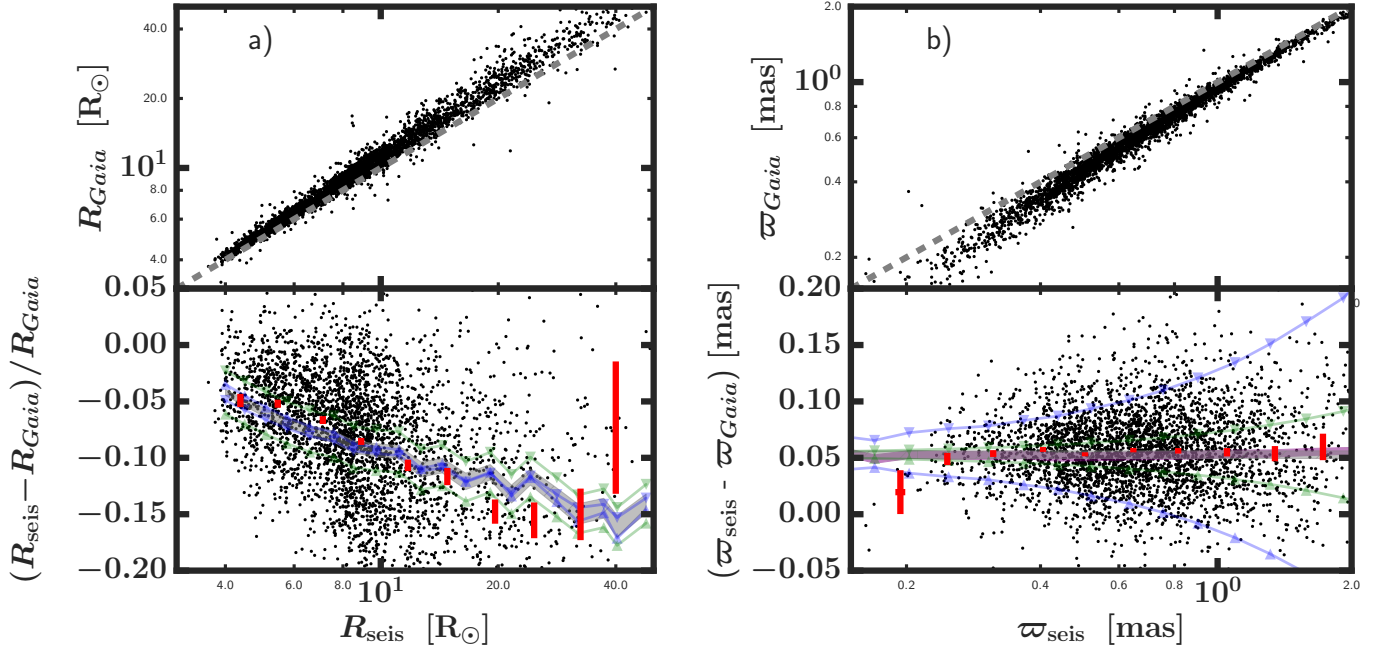


**Figure 3:** Fractional difference in *Gaia* and APOKASC-2 radii, as a function of APOKASC-2 radii (a) and difference in *Gaia* and astroseismic parallax, as a function of astroseismic parallax. In the radius panel (a), the grey band indicates the best-fitting  $1\sigma$  model, which only allows for an offset in the *Gaia* parallax (Equation 16). In the parallax panel, the purple band indicates a model that allows for color and  $G$  terms in the *Gaia* parallax error (Equation 8), with  $\pm 1\sigma$  in the constant offset, and  $\pm 0.5\sigma$  in the color and  $G$  terms. The observed data (black) and binned median (red error bars) are well-described by a constant offset of  $c$  (grey band). Shown also are models describing how the binned medians of the data (red error bars) would appear in the presence of  $\pm 100K$  in the APOGEE temperature scale (blue) and  $\pm 2\%$  in the radius scaling relation (Equation 3; green). See text for details.

in prep.). As we mention in §1, a trend with parallax was present in TGAS parallaxes, as well.

## 6. CONCLUSIONS

With a sample of nearly 3500 first-ascent giants in the APOKASC-2 catalogue, we infer a systematic error in the *Gaia* parallaxes of  $52.8 \pm 2.4(stat.) \pm 1(syst.)\mu\text{as}$ , in the sense that *Gaia* parallaxes are too small. All indications are that the zero-point error is position-, magnitude, and color-dependent (L18), so we do not advise to use our offset out-of-the-box. Our work does, however, serve as a useful reference for other studies needing to account for the zero-point error in their work.

In this sense, we have confidence in our result because of agreement with the zero-point parallax offset of  $29\mu\text{as}$  that L18 finds for a sample of nearly 600,000 quasars from AllWISE (Secrest et al. 2015), in the same sense that we find. Arenou et al. (2018) computes offsets using more than 200,000 stars from 29 sources, ranging from *Hipparcos* (van Leeuwen 2007b) to the spectrographic survey LAMOST (Luo et al. 2015), with significant offsets ranging from  $\approx 10 - 100\mu\text{as}$ , also in the sense that *Gaia* parallaxes are too small. Finally, Riess et al. (2018)

corroborates the findings, citing an offset of  $46 \pm 13\mu\text{as}$ . Though our offset is larger in an absolute sense than found by L18 and Riess et al. (2018) (yet well within the range Arenou et al. 2018 finds), Figure 7 in L18, which shows the zero-point offset in the AllWISE quasar sample as a function of ecliptic latitude, suggests that the *Kepler* field, at  $\sim 64^\circ$ , should exhibit the highest offset at  $\sim 50\mu\text{as}$ .

We leave the reader with the following conclusions:

1. For studies using *Gaia* parallaxes of populations of giants in the *Kepler* field, we think our estimate of  $\varpi_{\text{seis}} - \varpi_{\text{Gaia}} = 52.8 \pm 2.4(stat.) \pm 1(syst.) - (150.7 \pm 22.7\mu\text{as})(\nu_{\text{eff}} - 1.5) - (4.21 \pm 0.77)(G - 12.2)\mu\text{as}$  should be valid, given the various tests provided in §5. In our sample, which has a range of  $\sim 0.2$  in  $\nu_{\text{eff}}$  and spans  $\sim 4$  magnitudes, the color and magnitude terms are appreciable.
2. It appears the offset is *Gaia* parallax-dependent, with an increase in the absolute zero-point error with decreasing parallax. This, however, could be due to selection effects of our sample or a breakdown in scaling relations for the most evolved gi-

Sample	$c$ [ $\mu\text{as}$ ]	$d$ [ $\mu\text{as}\mu\text{m}$ ]	$e$ [ $\mu\text{as}\text{mag}^{-1}$ ]	$\chi^2/\text{dof}$	$N$
$b < 15^\circ$	$53.7 \pm 2.8$	$-125.5 \pm 26.4$	$-4.10 \pm 0.89$	0.946*	2532
$\ell < 73^\circ$	$51.6 \pm 4.4$	$-34.9 \pm 39.2$	$-3.56 \pm 1.41$	1.092*	891
$b > 15^\circ$	$53.3 \pm 3.2$	$-191.8 \pm 42.2$	$-4.41 \pm 1.48$	1.116**	942
$\ell > 73^\circ$	$53.1 \pm 2.6$	$-203.8 \pm 27.3$	$-4.57 \pm 0.90$	0.975	2584
$\varpi_{\text{Gaia}} > 1\text{mas}$	$46.0 \pm 5.7$	$-255.7 \pm 146.3$	$-13.25 \pm 3.82$	0.583*****	555
$\sigma_{\varpi_{\text{Gaia}}}/\varpi_{\text{Gaia}} < 0.05$	$53.1 \pm 2.3$	$-215.3 \pm 39.7$	$-5.92 \pm 1.00$	0.781*****	2640
RC	$50.2 \pm 2.5$	$-315.2 \pm 49.3$	$0.79 \pm 1.07$	0.666*****	2587
RGB	$52.8 \pm 2.4$	$-150.7 \pm 22.7$	$-4.21 \pm 0.77$	1.007	3475

**Table 1:** *Gaia* zero-point errors,  $c$ , and their errors inferred from various APOKASC-2 populations when fitting with Equation 8. See text for details. Asterisks denote the level of discrepancy with the expected  $\chi^2$  given the degrees of freedom,  $N - 3 - 1$ , with one asterisk for each  $\sigma$  in the significance of the discrepancy, capped at  $5\sigma$ . Our preferred value is from the “RGB” sub-sample. We estimate a systematic error in  $c$  due to the choice of a function to describe *Gaia* parallax spatial covariance at the level of  $\pm 1\mu\text{as}$ .

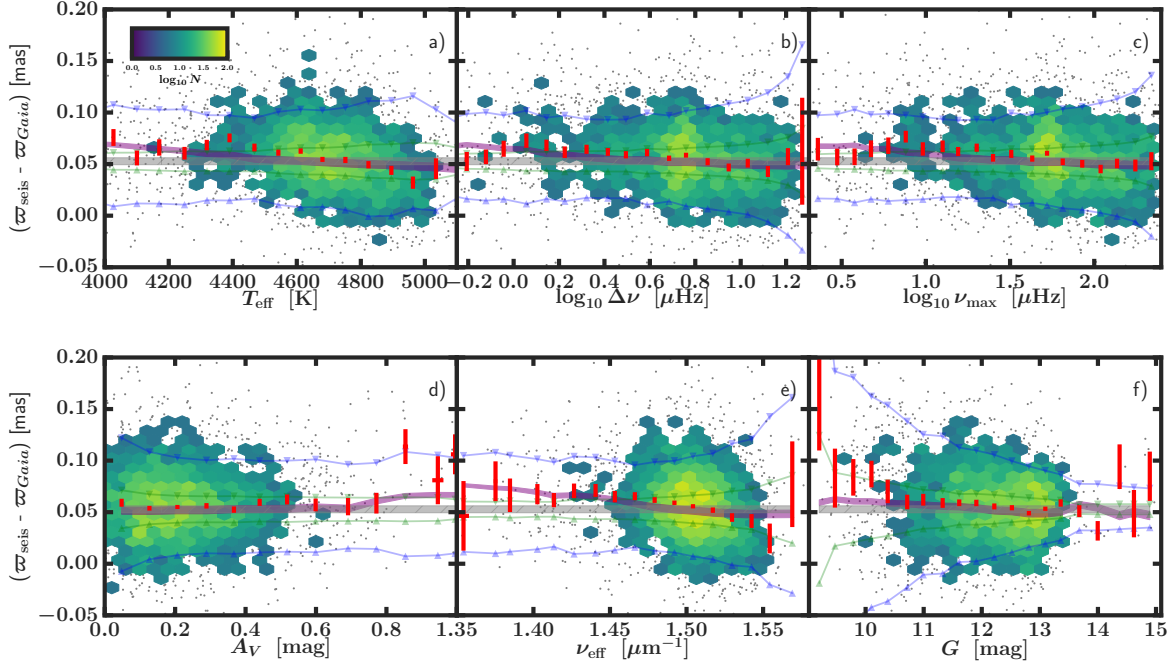


**Figure 4:** Difference in *Gaia* and asteroseismic parallax, as a function of  $T_{\text{eff}}$  (a),  $\Delta\nu$  (b),  $\nu_{\text{max}}$  (c),  $A_V$  (d),  $\nu_{\text{eff}}$  (e), and  $G$  (f). In general, the observed data (black) and binned median (red error bars) are well-described by a constant offset of  $c$  (grey band), but better described by a model that allows for color and  $G$  terms in the *Gaia* parallax error (purple band; with  $\pm 1\sigma$  in the constant offset, and  $\pm 0.5\sigma$  in the color and  $G$  terms). Shown also are predicted trends due to errors of  $\pm 100\text{K}$  in the APOGEE temperature scale (blue) and  $\pm 2\%$  in the radius scaling relation (Equation 3; green). See text for details. Errors on  $G$ -band magnitude have been set to 1%. The density of points per bin is denoted by the color bar in panel a.

- ants in our sample, and we will explore this in more detail in future work.
- There are only insignificant differences in the *Gaia* zero-point error due to extinction in the *Kepler* field.
- We have provided an offset for our RC population of  $50.2 \pm 2.5\mu\text{as}$ , which differs from our preferred estimate using RGB stars primarily due to systematic errors in the RC asteroseismic radius scale due to the fact that the APOKASC-2 radii were cal-

ibrated on open RGB stars, and not red clump stars. The offset for the clump remains of interest to studies planning to use *Gaia* DR2 parallaxes for *Kepler* red clump stars.

5. Our spatial covariance model of the DR2 parallaxes in the *Kepler* field likely needs revision, which we will quantify in future work. At this point, there are uncertainties on the parallax zero-point error due to not knowing the precise nature of the spatial correlations, which are on the order of  $\pm 1\mu\text{as}$ .

The color term to describe the zero-point error that we estimate may represent variations in the asteroseismic scaling radius scale with evolutionary state, though a color term is certainly expected in the *Gaia* parallax zero-point (Lindgren et al. 2018; Arenou et al. 2018). We will investigate this and estimate the spatial dependence of *Gaia* parallax errors in a forthcoming paper on tests of scaling relations as a function of evolutionary state.

M. H. P. and J. Z. acknowledge support from NASA grants 80NSSC18K0391 and NNX17AJ40G. D. H. acknowledges support by the National Science Foundation (AST-1717000) and the National Aeronautics and Space Administration under Grants NNX14AB92G and NNX16AH45G issued through the Kepler Participating Scientist Program and the K2 Guest Observer Program. D. S. is the recipient of an Australian Research Council Future Fellowship (project number FT1400147). Parts of this research were conducted by the Australian Research Council Centre of Excellence for All Sky Astrophysics in 3 Dimensions (ASTRO 3D), through project number CE170100013.

This work has made use of data from the European Space Agency (ESA) mission *Gaia* (<https://www.cosmos.esa.int/gaia>), processed by the *Gaia* Data Processing and Analysis Consortium (DPAC, <https://www.cosmos.esa.int/web/gaia/dpac/consortium>). Funding for the DPAC has been provided by national institutions, in particular the institutions participating in the *Gaia* Multilateral Agreement.

Funding for the Sloan Digital Sky Survey IV has been provided by the Alfred P. Sloan Foundation, the U.S. Department of Energy Office of Science, and the Participating Institutions. SDSS acknowledges support and resources from the Center for High-Performance Computing at the University of Utah. The SDSS web site is [www.sdss.org](http://www.sdss.org). SDSS is managed by the Astrophysical Research Consortium for the Participating Institutions of the SDSS Collaboration including the Brazilian Participation Group, the Carnegie Institution for Science, Carnegie Mellon University, the Chilean Participation Group, the French Participation Group, Harvard Smithsonian Center for Astrophysics, Instituto de Astrofísica de Canarias, The Johns Hopkins University, Kavli Institute for the Physics and Mathematics of the Universe (IPMU) / University of Tokyo, Lawrence Berkeley National Laboratory, Leibniz Institut für Astrophysik Potsdam (AIP), Max-Planck-Institut für Astronomie (MPIA Heidelberg), Max-Planck-Institut für Astrophysik (MPA Garching), Max-Planck-Institut für Extraterrestrische Physik (MPE), National Astronomical Observatories of China, New Mexico State University, New York University, University of Notre Dame, Observatório Nacional / MCTI, The Ohio State University, Pennsylvania State University, Shanghai Astronomical Observatory, United Kingdom Participation Group, Universidad Nacional Autónoma de México, University of Arizona, University of Colorado Boulder, University of Oxford, University of Portsmouth, University of Utah, University of Virginia, University of Washington, Uni-

versity of Wisconsin, Vanderbilt University, and Yale University.

## REFERENCES

- Andrae, R., Fouesneau, M., Creevey, O., et al. 2018, ArXiv e-prints, arXiv:1804.09374
- Arenou, F., Luri, X., Babusiaux, C., et al. 2018, ArXiv e-prints, arXiv:1804.09375
- Bailer-Jones, C. A. L. 2015, *PASP*, 127, 994
- Bailer-Jones, C. A. L., Andrae, R., Arcay, B., et al. 2013, *AAP*, 559, A74
- Bedding, T. R., Huber, D., Stello, D., et al. 2010, *ApJL*, 713, L176
- Borucki, W. J., Koch, D., Basri, G., et al. 2010, *Science*, 327, 977
- Brogaard, K., Jessen-Hansen, J., Handberg, R., et al. 2016, *Astronomische Nachrichten*, 337, 793
- Brown, T. M., Gilliland, R. L., Noyes, R. W., & Ramsey, L. W. 1991, *ApJ*, 368, 599
- Brown, T. M., Latham, D. W., Everett, M. E., & Esquerdo, G. A. 2011, *AJ*, 142, 112
- Casertano, S., Riess, A. G., Bucciarelli, B., & Lattanzi, M. G. 2017, *AAP*, 599, A67
- Davies, G. R., Lund, M. N., Miglio, A., et al. 2017, *AAP*, 598, L4
- De Ridder, J., Molenberghs, G., Eyer, L., & Aerts, C. 2016, *AAP*, 595, L3
- De Ridder, J., Barban, C., Baudin, F., et al. 2009, *Nature*, 459, 398
- Evans, D. W., Riello, M., De Angeli, F., et al. 2018, ArXiv e-prints, arXiv:1804.09368
- Flower, P. J. 1996, *ApJ*, 469, 355
- Frandsen, S., Lehmann, H., Hekker, S., et al. 2013, *AAP*, 556, A138
- Gaia Collaboration, Brown, A. G. A., Vallenari, A., et al. 2018, ArXiv e-prints, arXiv:1804.09365
- Gaia Collaboration, Prusti, T., de Bruijne, J. H. J., et al. 2016a, *AAP*, 595, A1
- . 2016b, *AAP*, 595, A1
- Gaulme, P., Jackiewicz, J., Appourchaux, T., & Mosser, B. 2014, *ApJ*, 785, 5
- Gaulme, P., McKeever, J., Jackiewicz, J., et al. 2016, *ApJ*, 832, 121
- González Hernández, J. I., & Bonifacio, P. 2009, *AAP*, 497, 497
- Hekker, S., Kallinger, T., Baudin, F., et al. 2009, *AAP*, 506, 465
- Huber, D., Ireland, M. J., Bedding, T. R., et al. 2012, *ApJ*, 760, 32
- Huber, D., Zinn, J., Bojsen-Hansen, M., et al. 2017, *ApJ*, 844, 102
- Jao, W.-C., Henry, T. J., Riedel, A. R., et al. 2016, *ApJL*, 832, L18
- Kjeldsen, H., & Bedding, T. R. 1995, *AAP*, 293, 87
- Lindegren, L., Lammers, U., Bastian, U., et al. 2016, *AAP*, 595, A4
- Lindegren, L., Hernandez, J., Bombrun, A., et al. 2018, ArXiv e-prints, arXiv:1804.09366
- Luo, A.-L., Zhao, Y.-H., Zhao, G., et al. 2015, *Research in Astronomy and Astrophysics*, 15, 1095
- Michalik, D., Lindegren, L., & Hobbs, D. 2015, *AAP*, 574, A115
- Miglio, A., Brogaard, K., Stello, D., et al. 2012, *MNRAS*, 419, 2077
- Mosser, B., Dziembowski, W. A., Belkacem, K., et al. 2013, *AAP*, 559, A137
- Neiswanger, W., Wang, C., & Xing, E. 2013, ArXiv e-prints, arXiv:1311.4780
- Pinsonneault, M. H., An, D., Molenda-Żakowicz, J., et al. 2012, *ApJS*, 199, 30
- Pinsonneault, M. H., Elsworth, Y. P., Tayar, J., et al. 2018, ArXiv e-prints, arXiv:1804.09983
- Riess, A. G., Casertano, S., Yuan, W., et al. 2018, ArXiv e-prints, arXiv:1804.10655
- Rodrigues, T. S., Bossini, D., Miglio, A., et al. 2017, *MNRAS*, 467, 1433
- Secrest, N. J., Dudik, R. P., Dorland, B. N., et al. 2015, *ApJS*, 221, 12
- Sesar, B., Fouesneau, M., Price-Whelan, A. M., et al. 2017, *ApJ*, 838, 107
- Sharma, S., Stello, D., Bland-Hawthorn, J., Huber, D., & Bedding, T. R. 2016, *ApJ*, 822, 15
- Skrutskie, M. F., Cutri, R. M., Stiening, R., et al. 2006, *AJ*, 131, 1163
- Stassun, K. G., & Torres, G. 2016a, *ApJL*, 831, L6
- . 2016b, *AJ*, 152, 180
- Stello, D., Huber, D., Bedding, T. R., et al. 2013, *ApJL*, 765, L41
- Stello, D., Compton, D. L., Bedding, T. R., et al. 2014, *ApJL*, 788, L10
- Ulrich, R. K. 1986, *ApJL*, 306, L37
- van Leeuwen, F. 2007a, *AAP*, 474, 653
- . 2007b, *AAP*, 474, 653
- White, T. R., Bedding, T. R., Stello, D., et al. 2011, *The Astrophysical Journal*, 743, 161
- Wright, E. L., Eisenhardt, P. R. M., Mainzer, A. K., et al. 2010, *AJ*, 140, 1868
- Yu, J., Huber, D., Bedding, T. R., et al. 2018, ArXiv e-prints, arXiv:1802.04455
- Zinn, J. C., Huber, D., Pinsonneault, M. H., & Stello, D. 2017, *ApJ*, 844, 166